Quaternary Research (2025), 1–12
doi:10.1017/qua.2024.49

Research Article

Dust pathways of the Songnen Plain, Northeast China in the last glacial period and their implications for ecological security

Yan Jiao[a,†], Yuanyun Xie[a,b,†], Yunping Chi[a,b], Lei Sun[a,b], Peng Wu[a], Zhenyu Wei[a], Haijin Liu[a], Yehui Wang[a] and Ruonan Liu[a]

[a]College of Geographic Science, Harbin Normal University, Harbin 150025, China and [b]Heilongjiang Province Key Laboratory of Geographical Environment Monitoring and Spatial Information Service in Cold Regions, Harbin Normal University, Harbin 150025, China

Abstract

Loess, a geologic record of dust, is an optimal archive for exploring paleoclimate and the paleo-dust path from source to sink. The dust path for the Songnen Plain, NE China, during the last glacial period has not been established. To address this, 63 surface sediment samples from the Northeast China Sandy Lands, i.e., Onqin Daga Sandy Land (OD), Horqin Sandy Land (HQ), Hulun Buir Sandy Land (HL), and Songnen Sandy Land (SN), and six samples from the last glacial loess in the Harbin area were collected for elemental geochemical analysis of the <10 μm fraction to quantitatively reconstruct the dust pathway using a frequentist model. The results show that these sandy lands have a distinct geochemical composition due to a control from markedly different provenances. The quantitative results indicate that the dust contribution of the southwestern SN to the Harbin loess is as high as 50.4–77.2%, followed by the OD and HQ (3.3–34.8%), the northwestern SN (0–36.8%), and the HL (0–8%). Notably, the dust contribution to the Harbin loess began to change considerably after ~46–41 ka BP, with a significant increase from 1.1% to 41.2% from the northwestern direction. Some ecological safety strategies are proposed to address dust pollution in the Harbin area.

Keywords: Northeast Sandy Lands, Songnen Plain, Harbin loess, dust path, source fingerprinting, geochemical analysis

INTRODUCTION

Atmospheric dust is an important part of the climate system, which has direct effects on radiation balance and hydrologic processes, and plays an important role in the global biogeochemical cycle and the Earth's climate system (Jickells et al., 2005; Forster et al., 2007; Mahowald et al., 2010). At the same time, loess, as an ancient dust accumulation, records information about the paleoclimate and paleoenvironment, and research on its provenance is crucial for understanding climate aridification, atmospheric circulation patterns, and monsoon evolution (Smalley, 1995; Liu and Ding, 1998; Chou et al., 2008; Maher et al., 2010; Bi et al., 2011).

Element geochemical methods have been extensively employed to discriminate the source and transportation processes of sediments (Grousset and Biscaye, 2005; Rao et al., 2006, 2011; Chen et al., 2007; Yang et al., 2007a; Du et al., 2018; Ding et al., 2021). However, traditional geochemical source-area tracing often uses several typical elements or element ratios (Liu and Yang, 2018; Shu et al., 2018; Jiang and Yang, 2019; Zhang et al., 2020, 2022), wherein this artificial selection may overlook specific elements (or element ratios) that are more suitable for a particular study. In addition, the results of source discrimination based on visual comparison are often highly biased, thus producing ambiguous source reconstructions. Recently, a frequentist model based on an R package analysis, a new sediment source fingerprinting technique recently used to quantitatively assess the relative contribution of potential source areas, has been successfully applied to quantitatively identify the sources of fluvial and aeolian sediments (García Comendador et al., 2021; Song et al., 2022). Therefore, the sediment source fingerprint model has great potential for revealing quantitative source information about dust sediments (Lizaga et al., 2020).

The Harbin loess, located on the easternmost margin of the Eurasian Loess belt, is a typical loess accumulation landform in NE China. Studying its provenance is of great significance for explaining the relationship between the geomorphology, climate, and dust accumulation on the Songnen Plain (Sun and Lu, 2007). The Northeast China Sandy Lands, located in the upwind area of the Harbin loess, are considered to be important potential source areas due to the characteristics of the near-source accumulation of aeolian loess (Kang et al., 2013; Xie et al., 2020a; Sun et al., 2022). Up to now, great progress has been made in the geochemical source tracing of most of the sandy lands in Central Asia and north China (Zhao et al., 2019; Xie et al., 2020b; Chen et al., 2021; Li L. et al., 2023), but data on the geochemical characteristics and provenance tracing of the sandy lands in NE China are still scarce. The few previous studies regarding dust source tracing in NE China focused on qualitative analysis (Wu et al., 2022; Liang et al., 2023), which is insufficient to explain the relative contributions of dust sources. In recent years, although some quantitative source works have been carried out on the loess in NE China (Wu et al., 2022, 2023), the works are limited to the

Corresponding authors: Y. Xie; Email: xyy0451@163.com; Y. Chi; Email: 1982cyp@163.com

[†]Joint first authors: Y. Jiao and Y. Xie.

Cite this article: Jiao Y, Xie Y, Chi Y, Sun L, Wu P, Wei Z, Liu H, Wang Y, Liu R (2025). Dust pathways of the Songnen Plain, Northeast China in the last glacial period and their implications for ecological security. *Quaternary Research* 1–12. https://doi.org/10.1017/qua.2024.49

<63 μm fraction. Specifically, dust particles of <10 μm can remain suspended in the upper atmosphere for extended periods and be transported over a long distance under the influence of upper atmospheric dynamics. Therefore, quantitative reconstruction of dust sources based on the <10 μm fraction can more effectively reveal information about the dust transportation in the upper atmosphere (Ding et al., 2000; Sun et al., 2004; Vandenberghe, 2013; Licht et al., 2016; Újvári et al., 2016).

In this study, surface sediments in the sandy lands (Onqin Daga Sandy Land, Horqin Sandy Land, Hulun Buir Sandy Land, and Songnen Sandy Land) in NE China were collected along with last glacial loess samples in NE China for geochemical analysis of the <10 μm fraction, with an aim to quantitatively reconstruct the high-altitude dust path of the Songnen Plain during the last glacial period. This study provides not only an important insight into the aeolian dust system in NE China, but also important theoretical support for the construction of regional ecological security.

REGIONAL SETTING

The Northeast Sandy Lands are located east of Inner Mongolia, southwest of Heilongjiang Province, and west of Jilin Province, China, and include the Onqin Daga Sandy Land (OD), the Horqin Sandy Land (HQ), the Hulun Buir Sandy Land (HL), and the Songnen Sandy Land (SN) (Fig. 1). The Northeast Sandy Lands are dominated by semifixed and fixed sand dunes, with fewer active dunes.

The OD is located on the southern side of the Xilin Gol grassland in central Inner Mongolia, covering an area of 52,000 km^2 with an average elevation of 1100 m (Yang et al., 2019). The HQ, at 62,432 km^2 in area, is the largest sandy land in China (Yang et al., 2012; Chen et al., 2022) and is located in the middle and lower reaches of the West Liaohe River in the southeast of Inner Mongolia. The West Liaohe River system connects the OD and the HQ from west to east. The HL, 7435 km^2 in area, is the highest latitude sandy land in China and is located in the western part of the Great Xing'an Range (Fig. 1). The HL is developed from an alluvial-lacustrine plain, with more than two-thirds of the area covered by river and lake sediments (Yang et al., 2019). The SN, 8356 km^2 in area, is located in the central and western parts of the Songnen Plain and is mainly distributed along the floodplains and terraces of the Nenjiang River and Songhua River (Qiu, 2008; Xie et al., 2020a). According to the direction of the prevailing winds and the possible dust source areas, the SN can be divided into two regions, northwest (SNNW) and southwest (SNSW). The SNNW is predominantly situated in the vicinity of the Nenjiang River basin, covering regions such

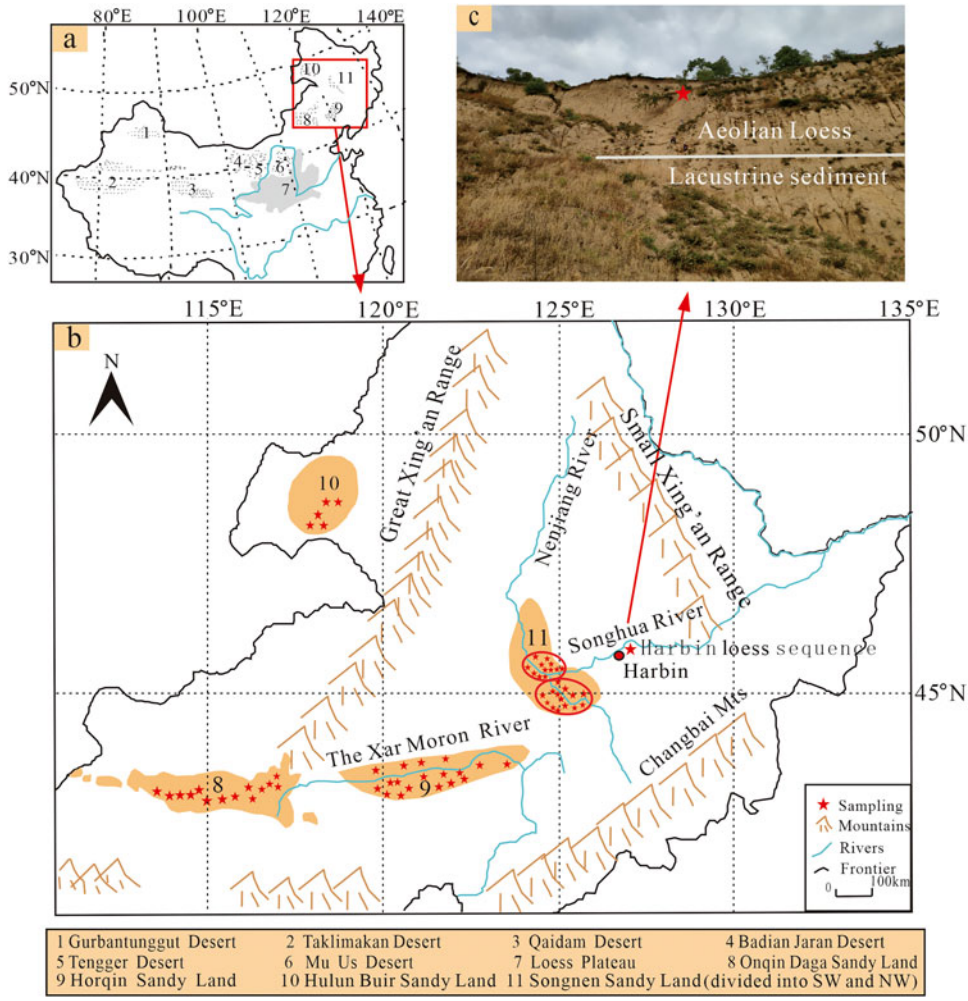

Figure 1. (a) Sketch map of desert distribution in northern China. (b) Sketch map of the Northeast Sandy Lands in China, showing location of the study area and sampling section sites. (c) Profile photograph of the Harbin loess section.

https://doi.org/10.1017/qua.2024.49 Published online by Cambridge University Press

as Dumeng, Qiqihar, Tailai, Zhenlai, and Baicheng. In contrast, the SNSW is predominantly located near the Songhua River basin, encompassing areas such as Changling, Qian'an, Zhaoyuan, Da'an, Songyuan, Fuyu, and Tongyu.

Harbin city is located in the northeast of the Songnen Plain, adjacent to the Zhangguangcai Range to the southeast and the Lesser Hinggan Mountains to the north, and has a semihumid temperate continental monsoon climate. The region is dominated by southwest winds in spring/summer and northwest winds in winter. The Harbin Huangshang loess sequence (HS, 45°47′N, 126°47′E) is located on the second level terrace of the Songhua River, about 16 km east of Harbin City, with an altitude of 180 m.

MATERIALS AND METHODS

Sampling

The fine-grained aeolian and fluvial sands can represent the average composition of large areas after being fully transported and mixed by wind and hydrodynamic forces (Xie et al., 2019). The samples taken in this study are aeolian and fluvial sands in origin. A total of 63 surface sediment samples were collected in areas far from urban areas, 14 from the OD, 18 from the HQ, 5 from the HL, and 26 from the SN. In order to explore the contribution of these sandy lands to regional dust in Harbin, six loess samples were collected from the HS loess profile, with sample ages spanning from the last glacial period to the Holocene (Table 1).

Experimental methods

The bulk samples taken from the field were dry-sieved (Gartzia-Bengoetxea et al., 2009) by passing the samples through 10 μm (1350 mesh) copper sieves, to attain <10 μm fraction subsamples for geochemical analysis. The glass fuse method was selected for major element analysis, and fusion glasses were prepared by mixing the sample with flux ($Li_2B_4O_7$) in the proportion 1:10 (Tamponi et al., 2003). Measurement was carried out via an X-ray fluorescence spectrometer (AL104, PW2404). The detection limit is ~0.01 wt%, and analytical precision (relative standard deviation) for major elements, except for Mn and P, is less than 1%. The analysis errors are generally less than 0.2% but with ±0.5% for SiO_2 and ±0.2% for Al_2O_3. Loss-on-ignition (LOI) was obtained by weighing before and after 1 h of heating at 950°C. The trace and rare earth element (REE) tests, following the acid dissolution method, which can maximize the extraction of chemical elements and reduce the error (Yang et al., 2007b), were performed on an inductively coupled plasma mass spectrometer (ICP-MS, Finnigan MAT, Element I). The Teflon bombs were first washed using aqua regia, ultra-pure HNO_3, and Milli-Q deionized water and placed on a heating plate at 120°C for 6 days. All samples were oven-dried, and 40 mg powder samples were placed in the Teflon cup and digested with ultra-pure acid. The samples were digested in 63% HNO_3 (1:1) and 48% HF at a high temperature (185 ± 5°C) following the four-step procedure detailed in Yang et al. (2007b) and Supplementary text S1. During the test process, standard samples, duplicate samples, and blank samples were interspersed for analysis to ensure the accuracy of the data, and the error was less than 2%. The element geochemical analysis was completed at the Key Laboratory of Mineral Resources in Western China (Gansu Province), Lanzhou University.

Table 1. Sampling depth of loess in Harbin and corresponding dating results.

Sample	HS1	HS2	HS3	HS4	HS5	HS6
Sampling depth (m)	3.5	3.25	2.3	2.05	1.05	0.46
Age (ka)	70	65	46	41	21	9.1

Principal component analysis

Principal component analysis (PCA) is a method of reducing the dimensions of original variables to several composite indicators. By combining variable indicators and adjusting combination coefficients, the new variables are made representative and independent of each other. The main calculation steps of PCA are as follows: first, the indicators and data are selected based on the research questions; second, the correlations of the indicators are tested to determine whether the original variables are suitable for factor analysis; finally, the correlations of the indicators are analyzed and calculated. The principal component and score calculation method of PCA was described thoroughly by Gu et al. (2012). PCA was performed in SPSS software (version 26).

Sediment source fingerprinting

The frequentist model is one of the most important methods for fingerprint identification of sediment sources (Adkison, 2009). In this study, 37 trace elements and 41 element ratios were selected as the geochemical fingerprint attributes for statistical analysis (see Supplementary Table 1). The sediment source fingerprinting method adopts a four-stage statistical program to trace the sediment source (Li et al., 2020; Hu et al., 2022). First, the bracket test of geochemical fingerprint attributes was performed to determine whether the average and extreme values of the loess properties are within the range of what could be observed by the source data, and then the test-passing properties were used for further research (Collins et al., 2010). Second, the non-parametric Kruskal-Wallis H-test was used to compare the difference of different provenance fingerprints in a potential provenance comparison (Gholami et al., 2020). This procedure removes tracers that do not show significant differences between at least two sediment sources. Third, the final composite fingerprints were further identified using step discriminant function analysis (DFA), which maximizes the differentiation between source regions while minimizing the number of geochemical fingerprints to provide the best differentiation between source regions (Collins et al., 1997). This function executes a stepwise forward variable selection for classification using the Wilks' lambda criterion, and selects the tracers based on the extent to which it decreases Wilks' lambda. At each step, the function includes the variable that minimizes the overall Wilks' lambda. And finally, based on the best composite fingerprint spectrum screened by the DFA discriminant function, a fingerprint analysis model was used to quantify the relative contribution of potential source areas to the loess samples (Li et al., 2020; Hu et al., 2022). The frequentist model is constructed in the R package program (version 4.0.3). Details of the standard linear multivariate mixing framework in the frequentist model can be referred to in the Supplementary text S2.

RESULTS

The geochemical composition of the <10 μm fraction of the aeolian and river sediments in the Northeast Sandy Lands (HQ, OD,

https://doi.org/10.1017/qua.2024.49 Published online by Cambridge University Press

HL, and SN), along with that of the Harbin loess sediments, is listed in Tables 2 and 3, respectively. More geochemical composition details are listed in Supplementary Tables 2 and 3, respectively.

Major elements

The major elements in the Northeast Sandy Lands are primarily SiO_2 and Al_2O_3, followed by Na_2O, Fe_2O_3, CaO, and K_2O, with slight contents of TiO_2, MnO, P_2O_5, and MgO. The distribution characteristics of the major elements in the sandy lands show overall homogeneity, with similar contents of SiO_2, Al_2O_3, MgO, Na_2O, K_2O, MnO, and P_2O_5, but the content of CaO in the OD is slightly higher than that in the other three sandy lands. Sandy lands with similar tectonic settings and regional geologic backgrounds may have indistinguishable source rocks and therefore indistinguishable major element compositions. Among the four sandy lands, CaO and TiO_2 contents have significant differences, with the highest CaO and lowest TiO_2 contents in the OD, the highest TiO_2 content in the HQ, and the lowest CaO content in the SN. Compared with upper continental crust (UCC; Taylor and McLennan, 1985), P_2O_5, MgO, and Na_2O are obviously depleted, K_2O, AL_2O_3, and Fe_2O_3 are slightly depleted, MnO and TiO_2 are significantly enriched, and SiO_2 remains relatively stable. (Fig. 2a).

Trace elements

The trace element composition of the <10 μm fraction in the Northeast Sandy Lands has similar Cr, V, Y, Th, and Rb contents, but differences in Co, Ni, Ta, U, Zr, and Hf (Fig. 2b). Specifically, the trace element patterns in the OD and the HQ are very similar. Compared with UCC, in the OD and HQ the contents of the transition trace elements (TTEs) Sc, Co, Ni, Zn, and Ga are moderately depleted, while V, Cr, and Cu are slightly enriched. For low field strength elements (LFSEs: Rb, Sr, Cs, Ba, Pb), Rb is slightly depleted, Sr is obviously depleted, Ba and Pb are slightly depleted in the HQ, and Ba and Pb are slightly enriched in the OD. For high field strength elements (HFSEs: Y, Zr, Nb, Hf, Ta, Th, U), Ta is obviously depleted, Zr, Hf, and Nb are slightly depleted, U is slightly enriched, and Y and Th are obviously enriched. In comparison to the other sandy lands, the content of TTEs in the HL is the lowest; for the LFSEs, Cs, Ba, and Pb are slightly enriched in the HL, while Rb and Sr are slightly depleted; for the HFSEs, Zr, Hf, U, Y, and Th are enriched in the HL, while Nb and Ta are slightly depleted. The SN is slightly enriched in Co, Cs, Ba, and Pb, and significantly enriched in Zr and Hf. The patterns of other elements are similar to those of the HQ (Fig. 2b).

Rare earth elements

The REE patterns in the surface sediments of the Northeast Sandy Lands are similar to those in UCC and post-Archean Australian shale (PAAS; Taylor and McLennan, 1985), with light rare earth (LREE) enrichment, heavy rare earth (HREE) depletion, and a significant negative Eu anomaly (Fig. 2c). The chondrite-normalized REE patterns of the Northeast Sandy Lands exhibit nearly parallel trends, with a steeper La–Eu curve and a flatter Eu–Lu curve. This suggests a relatively higher enrichment of LREEs over HREEs. The total amounts of REEs (ΣREE) in the HL, OD, HQ, and SN are 167–513 (260), 134–335 (216), 145–679 (271), and 194–388 (248), respectively, which is significantly higher than UCC (146) and PAAS (185). The Eu/Eu* values of all the sediments in the sandy lands are below 1, indicating prominent negative Eu anomalies. Their Ce/Ce* values are ∼0.95, suggesting a slight negative anomaly.

Sediment source fingerprinting

After the screening by the frequentist model program, a total of 14 tracers were ultimately determined, including Cr, Co, Zn, Ga, Zr, Hf, Y/Nb, Th/Ta, Y/Ta, Zr/Ta, Hf/Ta, Nb/Ta, Zr/Hf, and Th/(LREE/HREE), for the discrimination of source fingerprinting. The quantitative results based on the frequentist model show that the SNSW is the dominant dust source (Table 4), accounting for 50.4–77.2% (with an average of 62.3%) of the dust contribution, while the OD + HQ, SNNW, and HL account for 3.3–34.8% (with an average of 18.2%), 0–36.8% (with an average of 16.6%), and 0–8% (with an average of 2.85%), respectively.

DISCUSSION

Geochemical characteristics of the Northeast Sandy Lands

In recent years, dimensional statistical analysis or PCA has been a common mathematical statistical analysis method, mainly using linear transformation for the comparison between samples, and is usually more effective in distinguishing the differences between different samples compared to the elemental ratio binary diagrams (Nie and Peng, 2014), thus being widely applied in

Table 2. The average concentrations (wt%) of major elements for the <10 μm fraction in the Northeast Sandy Lands and Harbin loess.

Samples	SiO_2	Al_2O_3	Fe_2O_3	MgO	CaO	Na_2O	K_2O	MnO	TiO_2	P_2O_5	LOI	FeO
HL	68.65	12.83	3.48	1.04	2.72	3.07	3.02	0.10	1.20	0.08	3.63	1.11
HQ	72.20	11.69	3.50	0.90	2.17	2.71	2.58	0.09	1.37	0.10	2.67	1.41
OD	67.32	11.35	3.72	1.23	4.69	2.44	2.36	0.09	1.03	0.12	5.62	1.25
SNNW	69.65	13.10	3.48	0.90	2.14	2.90	2.82	0.10	0.98	0.10	0.74	3.78
SNSW	65.00	13.67	4.79	1.38	2.99	2.50	2.69	0.09	0.97	0.13	0.94	5.75
HS	65.95	14.91	4.85	1.46	1.51	2.13	2.75	0.08	0.66	0.13	4.84	0.93

Major elements without recalculation on a volatile-free basis.
Total iron as Fe_2O_3.
Abbreviations: HL, Hulun Buir Sandy Land; HQ, Horqin Sandy Land; OD, Onqin Daga Sandy Land; SNNW, northwestern area of the Songnen Sandy Land; SNSW, southwestern area of the Songnen Sandy Land; HS, Harbin Loess.

https://doi.org/10.1017/qua.2024.49 Published online by Cambridge University Press

Table 3. The average concentrations (ppm) of trace elements and REE for the <10 μm fraction in the Northeast Sandy Lands and Harbin loess.

Samples	Sc	V	Cr	Co	Ni	Cu	Zn	Ga	Rb	Sr	Y	Nb	Cs	Ba	Ta	Pb	Th	U	Zr	Hf	La	Ce	Pr	Nd	Sm	Eu	Gd	Tb	Dy	Ho	Er	Yb	Lu	Li	Be
HL	10.47	69.10	61.62	8.14	14.60	23.68	57.90	16.18	96.46	295.40	37.08	23.04	4.63	693.20	1.96	20.50	18.64	4.01	535.60	14.97	55.00	107.82	12.62	48.20	8.52	1.42	7.46	1.31	6.39	1.31	3.77	4.88	0.69	15.10	2.29
HQ	10.46	77.34	57.68	7.22	14.48	27.49	58.36	13.88	93.29	209.61	34.54	21.87	3.92	579.94	1.33	20.19	21.96	3.70	199.19	6.70	58.43	109.02	13.92	52.83	9.79	1.36	7.93	1.28	6.58	1.26	3.60	4.20	0.60	16.79	1.86
OD	8.74	79.36	57.00	9.21	19.06	34.19	54.11	12.79	82.97	244.21	28.69	16.92	4.45	601.50	1.31	20.61	16.39	3.06	178.56	5.68	46.01	87.25	10.75	41.64	7.81	1.23	6.48	1.07	5.50	1.05	3.04	3.36	0.48	19.96	1.64
SNNW	10.39	84.41	67.40	13.87	19.71	30.49	61.20	16.94	96.66	291.43	37.57	20.75	4.58	650.43	1.65	22.86	17.10	3.65	635.86	16.68	50.79	104.74	11.87	44.64	8.19	1.47	7.20	1.27	6.74	1.29	3.98	4.57	0.67	22.84	2.16
SNSW	11.86	80.79	65.75	12.27	22.93	27.41	77.22	18.46	101.12	272.15	31.71	24.94	6.19	586.15	2.02	23.97	15.16	2.67	372.23	10.51	44.73	91.48	10.36	40.54	7.51	1.29	6.60	1.09	5.86	1.17	3.27	3.85	0.55	24.48	2.37
HS	9.03	105.17	79.44	13.02	37.74	37.67	72.93	19.39	66.67	142.69	26.00	19.62	5.62	429.22	1.31	20.76	10.72	2.01	285.75	7.87	29.14	57.84	7.26	28.15	5.60	1.06	4.98	0.83	4.61	0.93	2.67	2.93	0.43	36.41	3.02

Abbreviations: HL, Hulun Buir Sandy Land; HQ, Horqin Sandy Land; OD, Onqin Daga Sandy Land; SNNW, northwestern area of the Songnen Sandy Land; SNSW, southwestern area of the Songnen Sandy Land; HS, Harbin Loess.

provenance study (Yang et al., 2010; Li L. et al., 2023; Li Y. et al., 2023). Some inactive elements (such as Ba, Zr, Hf, Li, Mo, etc.) are very stable in the process of weathering, denudation, transport, and sedimentation, and are transported almost completely from the source region into the sedimentary record; therefore, the properties of the parent rock are well preserved (Dehghani et al., 2018). In this study, the inactive element ratios Ba/Pb, Zr/Hf, Li/Be, and Mo/Cd of the samples were selected as initial variables for PCA analysis. In the PCA diagram (Fig. 3a), three separate areas are discernible—HL, SN, and a combination of OD and HQ—based on their differences in geochemical composition. Notably, the OD overlaps well with the HQ, and additionally, this is also the case for the SNNW and the SNSW despite slight differences in the geochemical composition, indicating their geochemical similarities. The scatter plots of immobile element ratios are the same as the PCA results (Figs. 3b and 3c), with four separate areas.

It is generally argued that provenance is a first-order control on the geochemical composition of sediments (Sun and Zhu, 2010; Chen and Li, 2013). The sediments in the OD and the HQ are deemed to ultimately originate from the Yanshan Mountains in the northern part of the North China Craton and from the Great Xing'an Range in the eastern part of the Central Asian Orogenic Belt (Xie et al., 2007; Liu et al., 2021), but with different proportions of contributions. Another important reason is transport by river and wind (Sun et al., 2004; Xie et al., 2014). The Xar Moron river, originating from the eastern edge of the OD, links the OD with the HQ. Accordingly, the fine-grained sediments in the OD are transferred by the river to the HQ. Concurrently, both the OD and the HQ are located in the dust transport path of the northwesterly wind, and they share similar dust source areas. These scenarios lead to the OD and the HQ having very similar compositions.

The Songnen Plain was formed by the alluvial processes of the Songhua River system (Qiu, 2008), and thus the sediments on the Songnen Plain are dominantly fed from the Great Xing'an Range via the Nenjiang River system, and the Changbai Mountains via the Jilin Songhua River system. In this scenario, the sediments in the northwestern part of the SN (i.e., SNNW), adjacent to the eastern side of the Great Xing'an Range, are mainly from the Great Xing'an Range, but the sediments in the southwestern part of the SN (i.e., SNSW) are more derived from the detritus supply from the Changbai Mountains (Xie et al., 2020b). However, the transition between the SNNW and the SNSW has a mixed source. This explains the fact that the two sandy lands are both independent and overlapping, as shown in Figure 3.

The geochemical disparities in the <10 μm fraction between the HL, SN, and a combination of the OD and HQ can be explained by their distinct sources, as also indicated by the <63 μm fraction in these sandy lands (Wu et al., 2022). The disparities in the geochemical composition in the potential dust sources contribute to the source-to-sink process study of dust on the Songnen Plain.

Quantitative contribution of the Northeast Sandy Lands to regional aeolian dust

Several conditions are usually required for loess accumulation, such as a continuous supply of sand and dust, wind transport capacity, and a suitable sink site (Pye, 1995; Qiu, 2008). Sandy lands and deserts are rich in dust, which can be transported by the wind to the downwind area under suitable geographic

https://doi.org/10.1017/qua.2024.49 Published online by Cambridge University Press

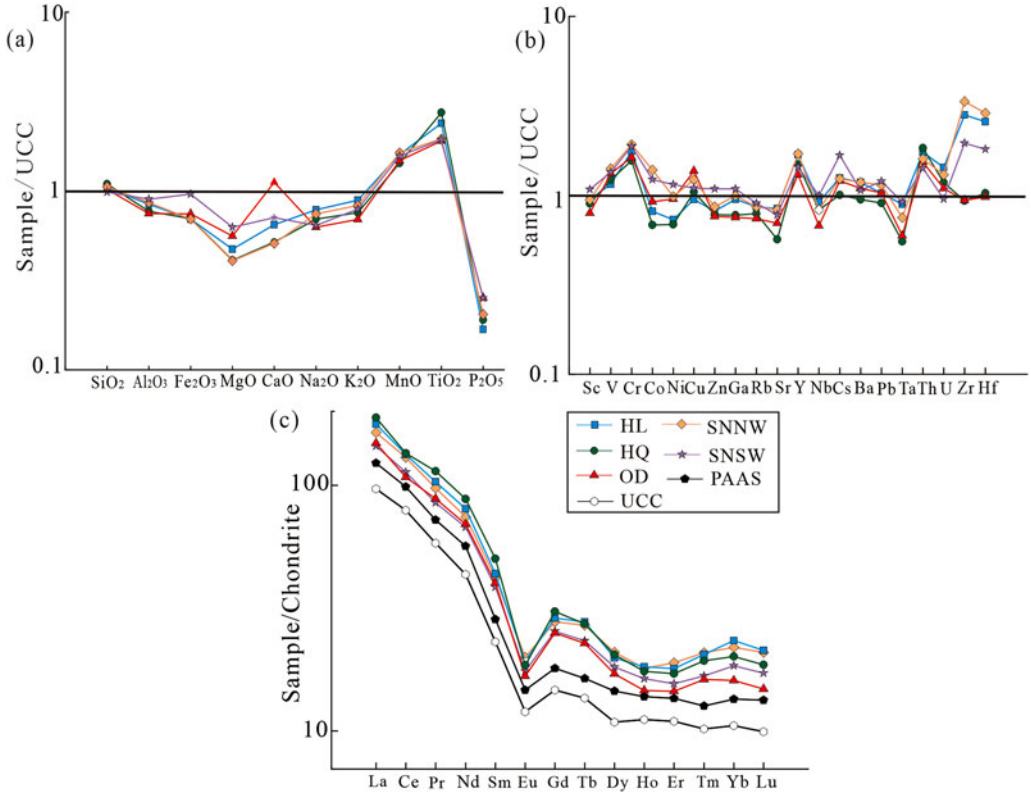

Figure 2. Normalized patterns for elements of the sediments in the Northeast Sandy Lands. (a) Upper continental crust (UCC)-normalized patterns for major elements; (b) UCC-normalized patterns for trace elements; (c) chondrite-normalized REE patterns for the studied sediments. Also shown are those of UCC and post-Archean Australian shale (PAAS) for comparison. UCC, PAAS, and chondrite values are from Taylor and McLennan (1985).

location, landform, and meteorological conditions (e.g., wind strength, wind direction, etc.). As a result, dust forming loess deposits usually comes from adjacent upwind arid or semiarid areas with a short transport distance (Sun, 2002; Chen et al., 2007; Li et al., 2009).

The Northeast Sandy Lands are located in the adjacent upwind area of the Harbin loess, and thus the near-source characteristics of aeolian loess make the Northeast Sandy Lands the potential source areas of the Harbin loess (Kang et al., 2013; Sun et al., 2022). The available provenance results of the <63 μm fraction of the Harbin loess have indicated the SN is the main dust source of the Harbin loess (Xie et al., 2020b; Wu et al., 2022; Liu et al., 2023). The <10 μm fraction of the Harbin loess is an environmentally sensitive endmember component (Sun et al., 2004; Wei et al., 2015; Du et al., 2020), and thus the quantitative dust source reconstruction based on the <10 μm component is of great significance for a deeper understanding of the aeolian dust system in the Northeast Plains.

Table 4. Quantitative reconstruction of the contribution of four source areas to the Harbin loess using the frequentist model. HS1–HS6 represent loess samples from Harbin.

Subzone	HS1	HS2	HS3	HS4	HS5	HS6
HL	0.9	0.0	1.1	8.0	4.9	2.2
HQ–OD	31.0	22.8	34.8	8.9	8.4	3.3
SNNW	0.0	0.0	0.0	26.7	36.3	36.8
SNSW	68.1	77.2	64.1	56.4	50.4	57.7

According to the results of the PCA, combined with the source discrimination diagram of immobile element ratios (Fig. 4), it can be observed that the Harbin loess samples are plotted far away from the HL and close to the SNSW, indicating that the SNSW is the main dust source area for the Harbin loess. Notably, two distinct regions have been identified within the Harbin loess (Fig. 4), indicating variable dust sources through time for the Harbin loess sediments.

The frequentist model, as one of the important means of sediment source fingerprinting, can provide the best distinction between source areas and quantify the relative contribution of potential source areas to sediments. Combined with the traditional provenance analysis method using the ratio of immobile elements, the sediment provenance can be comprehensively assessed (Xie and Chi, 2016; García Comendador et al., 2021; Song et al., 2022). Therefore, the quantitative source reconstruction of the sources of the Harbin loess using a frequentist model, combined with the source identification diagram composed of immobile element ratios, can comprehensively evaluate whether the Northeast Sandy Lands are the potential source areas of the Harbin loess and determine their relative contributions.

In order to more accurately determine which region contributes the most to the aeolian dust, the Northeast Sandy Lands need to be divided into several distinct regions before quantitative source reconstruction (Wu et al., 2023). Based on qualitative analysis results, the sandy lands are overall divided into four regions, as also reflected in the linear discriminant analysis (LDA) plot

https://doi.org/10.1017/qua.2024.49 Published online by Cambridge University Press

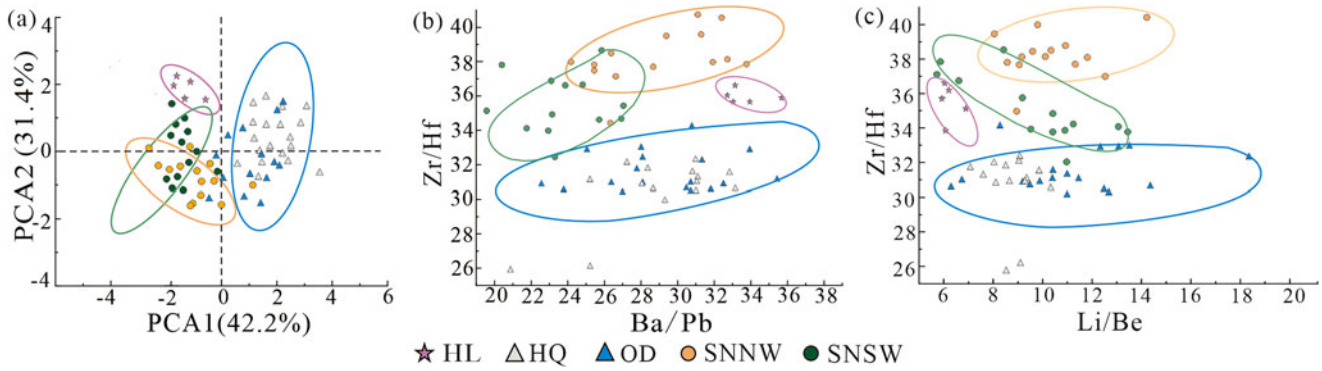

Figure 3. Discriminant diagrams showing geochemical differences in the Northeast Sandy Lands.

(Fig. 5). The LDA plot reveals a high overlap between the OD and HQ, with a clear difference between the SNSW and the SNNW. Therefore, the Northeast Sandy Lands are ultimately divided into the HL, SNSW, SNNW, and OD + HQ regions. In this contribution, 37 trace elements and 41 element ratios of the sediments from both the potential source areas and Harbin loess were selected as fingerprint attributes for statistical analysis of source fingerprints. The frequentist model first excluded the geochemical source fingerprint data outside the lowest and highest values of the potential source areas, and thus the four geochemical fingerprints Cu, Nb, Eu/Eu*, and Cr/Ni did not pass the range test. Secondly, 11 tracers, V, Mo, Ta, Ce/Ce*, Gd, Yb/N, U/Nb, U/Ta, Th/Sc, Th/U, and Cr/V, which failed the Kruskal-Wallis H-test and had no significant difference between source regions, were excluded from the original data set. Finally, the DFA discriminant function was used for variable selection, which maximizes the difference between source regions and minimizes the number of geochemical fingerprints. After systematic data screening, a total of 14 tracers such as Cr, Co, Zn, Ga, Zr, Hf, Y/Nb, Th/Ta, Y/Ta, Zr/Ta, Hf/Ta, Nb/Ta, Zr/Hf, and Th/(LREE/HREE) were identified for source fingerprinting.

The quantitative reconstruction results of the frequentist model indicate that the fingerprint characteristics of geochemical elements can effectively quantify the four source regions, and that

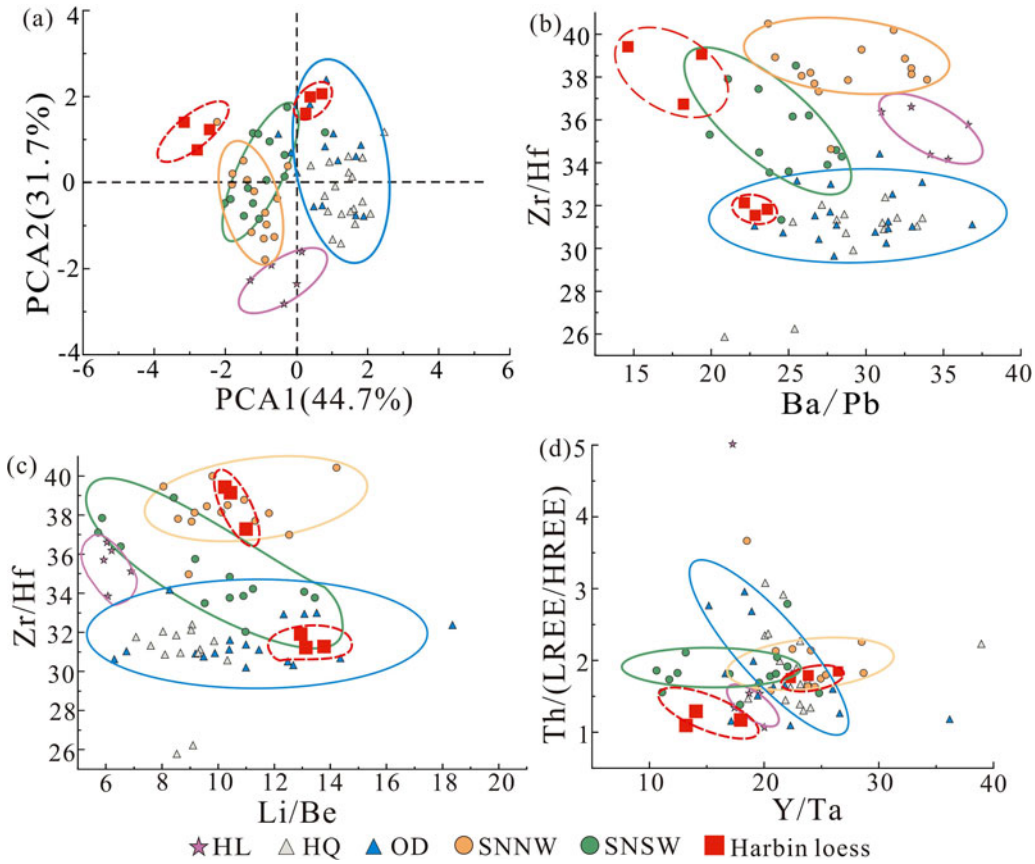

Figure 4. Provenance discrimination diagrams involving immobile elements of the Northeast Sandy Lands, showing the closer geochemical affinity of the loess in Harbin with the southwestern Songnen Sandy Land.

https://doi.org/10.1017/qua.2024.49 Published online by Cambridge University Press

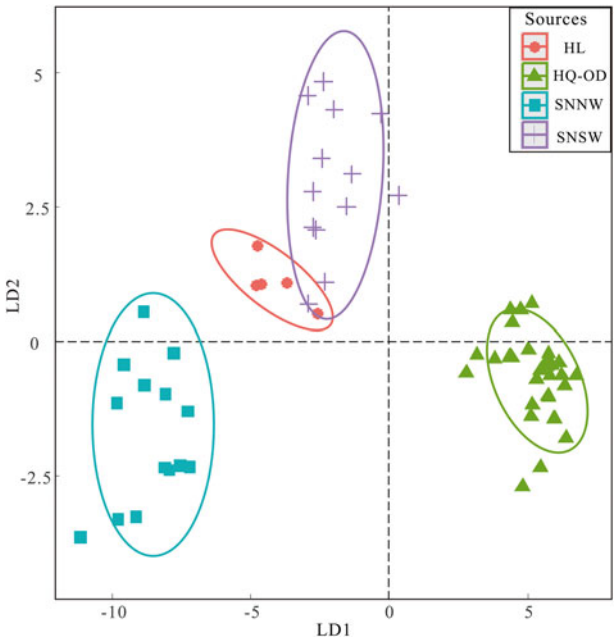

Figure 5. Linear discriminant analysis (LDA) plots of trace element geochemical data from four source areas of the target sediments with 95% confidence ellipses, using fingerprint properties tested by conservation, the Kruskal-Wallis H test, and the DFA test.

the dust contributions from the source areas have changed significantly since about 41 ka BP (Table 4). Before 41 ka BP, the SNSW dominates dust contribution to the Harbin loess (69.8%), followed by the OD + HQ (29.5%), with almost no dust contribution from the HL and SNNW. These findings indicate that the provenances of the Harbin loess are marked by the mixed accumulation of two endmembers, with the SNSW as the proximal source and the OD + HQ as the distal source. This result matches well with the quantitative results of the <63 μm fraction (Wu et al., 2023), but the only difference is that the near-source contribution (79%) of the <63 μm fraction is slightly larger than that (69.8%) of the <10 μm fraction. This consistency points to the fact that loess is a mixture of distal sources (Li et al., 2018; Zhang et al., 2018; Zeng et al., 2021), and the coarser loess in the glacial period has more near-source contributions, while the finer paleosol in the interglacial period has more far-source contributions (Prins et al., 2007; Miyazaki et al., 2016). After 41 ka BP, however, the abrupt and significant addition of dust contributions from the SNNW, ranging from 0 to 33%, is accompanied by the moderate reductions from the SNSW (ranging from 69.8 to 54.8%) and the OD + HQ (ranging from 29.5 to 6.9%), although the SNSW remains the dominant near-source contribution. The variations in the relative contribution of the dust sources to the Harbin loess are likely to be in response to the variations in climate (e.g., enhanced East Asian winter monsoon) and wind regimes (e.g., glacial–interglacial cycles) (Wu et al., 2023).

Dust path of the Songnen Plain during the last glacial period

The loess-paleosol sequences in the Chinese Loess Plateau are the products of the East Asian monsoon climate and offer a valuable archive for the reconstruction of past atmospheric circulation (An et al., 1991; Lu and An, 1998; An, 2000). The loess units were deposited by the transport of the winter monsoon during glacial periods in which an intensified winter monsoon prevailed, and the paleosols developed by pedogenesis during interglacial periods that were characterized by an enhanced summer monsoon and a relatively weakened winter monsoon (Liu and Ding, 1998; Sun, 2002).

The quantitative result of the Harbin loess provenance analysis provides direct clues about the dust path on the Songnen Plain linked to the atmospheric circulation pattern during that time. On the Songnen Plain, the wind regime associated with dust transport dominantly occurs in spring when the modern prevailing winds are southwesterly (occupying 85.7%), northwesterly (11.1%), and easterly (Xie et al., 2014). The annual dominant wind direction is southwesterly (Xie et al., 2020b). Accordingly, based on the modern prevailing winds, two different atmospheric circulation patterns on the Songnen Plain have been used to explain the transport and deposition of the loess deposits in NE China (Xie and Chi, 2016; Xie et al., 2018). Specifically, on the Songnen Plain, northwesterly winds were dominant in the glacial period, followed by southwesterly winds, while the circulation pattern in the interglacial period was dominated by southwesterly winds, which is also the main dynamics for spring dust-storm events (Xie et al., 2018).

The results of quantitative dust provenance reconstruction reveal a SW-direction dust path for the Harbin loess deposits, indicating that the southwesterly winds are the main driving force of dust transport on the Songnen Plain. This dust route is consistent with the annual dominant wind direction on the Songnen Plain. However, this route is at odds with the understanding that the loess was transported by the near-surface winter monsoon (northwesterly) during the last glacial period (Fig. 6; e.g., Liu, 1966; Sun, 2002; Sun et al., 2022). This means a decoupling between the wind regime and the dust path on the Songnen Plain during the last glacial period. The differences between the topography and ecological environment of the source areas likely explain this decoupling. Large areas of exposed detrital sediments, vegetation cover, and soil moisture are considered important factors in controlling dust emissions (Yue et al., 2005). Specifically, the SNNW has higher vegetation coverage (Wang and Du, 2018; Zhao and Song, 2021), which significantly reduces dust emissions, and its sand-fixing capacity is much higher than that of the SNSW (Xie et al., 2018). However, even during the glacial period dominated by northwesterly winds, the sparse vegetation coverage and large areas of exposed detrital sediments in the SNSW increased the availability of dust. In addition, the SW-direction source areas (i.e., the HQ, OD, and SNSW) have a flat topographic relief, and dust transport is not affected by topographic factors. In contrast, dust from the HL cannot reach the Harbin area due to the topographic barrier of the Great Xing'an Range (Xie et al., 2019; Sun et al., 2020).

An alternative dust route was identified on the Songnen Plain after ~46 ka to 41 ka (Fig. 6), and this route responded to the dynamic direction of the East Asian winter monsoon. The winds from the northwest intensified along with the reinforcement of the East Asian winter monsoon at that time (Gong et al., 2015), thereby causing the dust source area in the northwest to contribute more fine dust to the Harbin loess. This finding resonates with the quantitative results of the <63 μm fraction in which a sudden increase in dust contribution from the northwest direction is observed during 47–41 ka (Wu et al., 2023). However, our results show that the fine-grained component receives dust contributions from the northwest direction for a longer period, continuing into the Holocene. We speculate that this may be related to the finer dust particles being more sensitive to climate

https://doi.org/10.1017/qua.2024.49 Published online by Cambridge University Press

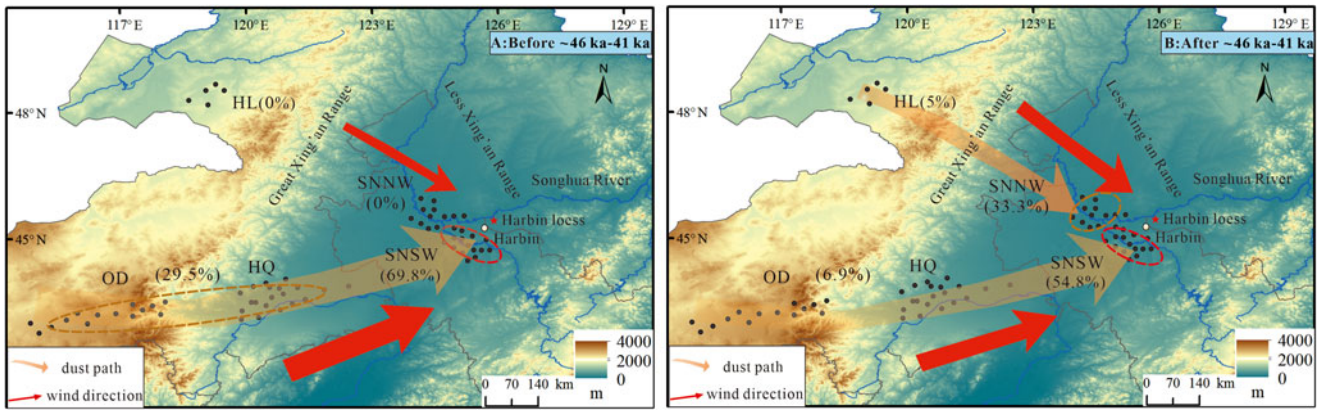

Figure 6. Schematic diagram showing the atmospheric circulation patterns and dust pathways on the Songnen Plain since the last glacial period; also shown are dust contributions from the sandy lands. The thick and thin orange arrows represent more and less dust contributions, respectively. The thick and thin red arrows represent the relatively stronger or weaker strength of the wind, respectively. The area marked by the dotted circle is the source area of the Harbin loess, with red and yellow dotted circles representing the primary and secondary source areas, respectively. The values in parentheses represent the average dust contribution percentage for the corresponding source area.

and provenance variations. In addition, the SN (including the SNSW and SNNW), as a neighboring source, provides advantageous dust material for the loess in Harbin under the conditions of the strengthened East Asian winter wind (~89%).

Implications for ecological security

As a very harmful meteorological phenomenon, the frequent dust-storm events in the Harbin area have caused serious damage to the ecological environment (Zhang et al., 2002). Dust storms are the main dust transport mechanism for loess formation (e.g., Xie and Chi, 2016), and the study of the dust transport pathway is of great practical significance to effectively prevent ecological environment problems and mitigate dust-storms.

The southwestern area of the SN is the main source of dust in the Harbin area, as mentioned before. Thus, the prevention and management of land desertification and the control of dust-storm events should first be focused on the SNSW, but not the SNNW, if limited human and financial resources are available. Concurrently, the work of desertification control and ecological environment restoration should be gradually carried out with permission. Based on the characteristics of the southwestern region of the SN and combined with the experience of large-scale sandy land management in NE China (e.g., the Horqin Sandy Land, Mu Us Sandy Land, Hulun Buir Sandy Land, etc.), the following basic measures are proposed for the ecological environment management of the southwestern region of the SN. Firstly, according to the patterns of vegetation succession in sandy lands, the optimal management model should be selected for different regions and ecological conditions. Secondly, priority should be given to preventing wind and fixing sand by increasing sand sealing efforts and forest cultivation, as well as expanding the area irrigated in the spring and improving farming practices to prevent wind erosion. Finally, by employing natural resources and reducing land uses such as agriculture, which can be highly destructive to the land, the full potential of the land can be utilized, leading to stable and coordinated ecosystem development. Efforts to prevent and control regional dust storms should extend beyond the affected areas. Greater attention should be given to managing the ecological environment in the potential source areas, in order to fundamentally improve the regional environmental conditions.

However, it is important to recognize that variable dust paths exist on the Songnen Plain and the northwest dust path, in operation during the Holocene, cannot be ignored. This poses a major challenge to ecological security construction in the Harbin area, thus requiring additional resources to be devoted to dust control in the northwest direction in addition to the existing efforts in the southwest direction. These results provide new insights for ecological governance, emphasizing the need for flexible governance strategies to better address the challenges of environmental governance.

CONCLUSIONS

The geochemical composition of the sediments (<10 μm fraction) in the Northeast Sandy Lands is obviously distinct due to a control from the markedly different source areas. The sediments of the HQ and OD have very similar geochemical compositions, due to the same sources and the combined effect of transportation by the Xar Moron river and the northwesterly winds.

Frequentist model quantitative reconstruction results show that the dust contribution of the SNSW to the Harbin loess is the highest, which can be as high as 77.2% before 41 ka BP. In this scenario, the contribution of the HL and SNNW is almost zero and the HQ + OD has the second largest dust contribution (22.8–34.8%). However, after 41 ka BP, the dust contribution from the northwest direction abruptly increases to much higher values (34.7–41.2%), accompanied by a decrease in the SNSW (50.4–57.7%) and the HQ + OD (3.3–8.9%).

The dust route on the Songnen Plain during the last glacial period is from the SW to NE before 41 ka BP, i.e., the dust has been transported along a route from the OD to the HQ and then to the SN. This dust route is consistent with the annual dominant wind direction on the Songnen Plain, but different from the northwesterly wind-dominated circulation pattern during the glacial period, which suggests a decoupling between circulation pattern and dust path on the Songnen Plain during the last glacial period. However, after ~46–41 ka, another dust route occurred in the northwest direction on the Songnen Plain, which is suggested to be in response to the intensified East Asian winter monsoon.

https://doi.org/10.1017/qua.2024.49 Published online by Cambridge University Press

The ecological environment management in the southwestern region of the Songnen Sandy Land should be strengthened in relation to the frequent dust-storm events in the Harbin area, and more attention should be paid to ecological environment management in the potential source area rather than in the occurrence area itself. However, the variable dust paths on the Songnen Plain pose a major challenge to dust ecological security construction in the Harbin area.

Supplementary material. The supplementary material for this article can be found at https://doi.org/10.1017/qua.2024.49

Acknowledgments. This study was financially supported by the Natural Science Foundation of Heilongjiang Province, China (Grant: ZD2023D003), and by National Natural Science Foundation of China (Grant: 42171006 and 41871013). The geochemical analysis was supported by the State Key Laboratory of Geological Processes and Mineral Resources, China University of Geosciences (Wuhan). Thanks to Xiaoyu Han, Peiyao Yang, Wanting Zhao, Ruitong Chang, Haodong Qi, and Jili Zeng for their participation in the discussion of the paper writing and assistance in sample pretreatment.

References

Adkison, M.D., 2009. Drawbacks of complex models in frequentist and Bayesian approaches to natural-resource management. *Ecological Applications* **19**, 198–205.

An, Z., 2000. The history and variability of the East Asian paleomonsoon climate. *Quaternary Science Reviews* **19**, 171–187.

An, Z.S., Kukla, G., Porter, S.C., Xiao, J.L., 1991. Late Quaternary dust flow on the Chinese loess plateau. *Catena* **18**, 125–132.

Bi, J., Huang, J., Fu, Q., Wang, X., Shi, J., Zhang, W., Huang, Z., Zhang, B., 2011. Toward characterization of the aerosol optical properties over Loess Plateau of Northwestern China. *Journal of Quantitative Spectroscopy and Radiative Transfer* **112**, 346–360.

Chen, B., Yang, X., Jiang, Q., Liang, P., Lattin Mackenzie, L., Zhou, Y., 2022. Geochemistry of aeolian sand in the Taklamakan Desert and Horqin Sandy Land, northern China: implications for weathering, recycling, and provenance. *Catena* **208**, 105769. https://doi.org/10.1016/j.catena.2021.105769.

Chen, J., Li, G., Yang, J., Rao, W., Lu, H., Balsam, W., Sun, Y., Ji, J., 2007. Nd and Sr isotopic characteristics of Chinese deserts: implications for the provenances of Asian dust. *Geochimica et Cosmochimica Acta* **71**, 3904–3914.

Chen, Q., Li, Z., Dong, S., Yu, Q., Zhang, C., Yu, X., 2021. Applicability of chemical weathering indices of eolian sands from the deserts in northern China. *Catena* **198**, 105032. https://doi.org/10.1016/j.catena.2020.105032.

Chen, Z., Li, G., 2013. Evolving sources of eolian detritus on the Chinese Loess Plateau since early Miocene: tectonic and climatic controls. *Earth and Planetary Science Letters* **371**, 220–225.

Chou, C., Formenti, P., Maille, M., Ausset, P., Helas, G., Harrison, M., Osborne, S., 2008. Size distribution, shape, and composition of mineral dust aerosols collected during the African Monsoon Multidisciplinary Analysis Special Observation Period 0: Dust and Biomass-Burning Experiment field campaign in Niger, January 2006. *Journal of Geophysical Research: Atmospheres* **113**, D00C10. https://doi.org/10.1029/2008JD009897.

Collins, A.L., Walling, D.E., Leeks, G.J., 1997. Fingerprinting the origin of fluvial suspended sediment in larger river basins: combining assessment of spatial provenance and source type. *Geografiska Annaler: Series A, Physical Geography* **79**, 239–254.

Collins, A.L., Zhang, Y., Walling, D.E., Grenfell, S.E., Smith, P., 2010. Tracing sediment loss from eroding farm tracks using a geochemical fingerprinting procedure combining local and genetic algorithm optimisation. *Science of the Total Environment* **408**, 5461–5471.

Dehghani, S., Moore, F., Vasiluk, L., Hale, B.A., 2018. The geochemical fingerprinting of geogenic particles in road deposited dust from Tehran metropolis, Iran: implications for provenance tracking. *Journal of Geochemical Exploration* **190**, 411–423.

Ding, J.N., Wu, Y.Q., Tan, L.H., Fu, T.Y., Du, S.S., Wen, Y.L., Li, D.W., 2021. Trace and rare earth element evidence for the provenances of aeolian sands in the Mu Us Desert, NW China. *Aeolian Research* **50**, 100683. https://doi.org/10.1016/j.aeolia.2021.100683.

Ding, Z.L., Rutter, N.W., Sun, J.M., Yang, S.L., Liu, T.S., 2000. Re-arrangement of atmospheric circulation at about 2.6 Ma over northern China: evidence from grain size records of loess-palaeosol and red clay sequences. *Quaternary Science Reviews* **19**, 547–558.

Du, H.R., Xie, Y.Y., Kang, C.G., Chi, Y.P., Wang, J., Sun, L., 2020. Grain size and geochemical characteristics of loess in Harbin and their implications for dust sources. *Deserts of China* **40**, 13. https://doi.org/10.7522/j.issn.1000-694X.2019.00046.

Du, S.S., Wu, Y.Q., Tan, L.H., 2018. Geochemical evidence for the provenance of aeolian deposits in the Qaidam Basin, Tibetan Plateau. *Aeolian Research* **32**, 60–70.

Forster, P., Ramaswamy, V., Artaxo, P., Berntsen, T., Betts, R., Fahey, D.W., Haywood, J., *et al.*, 2007. Changes in atmospheric constituents and in radiative forcing. In: Solomon, S., Qin, D., Manning, M., Chen, Z., Marquis, M., Averyt, K.B., Tignor, M., Miller, H.L. (Eds.), *Climate Change 2007: The Physical Science Basis. Contribution of Working Group I to the Fourth Assessment Report of the Intergovernmental Panel on Climate Change*. Cambridge University Press, Cambridge, pp. 129–234.

García Comendador, J., Martínez Carreras, N., Fortesa, J., Company, J., Borràs, A., Estrany, J., 2021. Combining sediment fingerprinting and hydro-sedimentary monitoring to assess suspended sediment provenance in a mid-mountainous Mediterranean catchment. *Journal of Environmental Management* **299**, 113593. https://doi.org/10.1016/j.jenvman.2021.113593.

Gartzia-Bengoetxea, N., González-Arias, A., Merino, A., de Arano, I.M., 2009. Soil organic matter in soil physical fractions in adjacent semi-natural and cultivated stands in temperate Atlantic forests. *Soil Biology and Biochemistry* **41**, 1674–1683.

Gholami, H., Rahimi, S., Fathabadi, A., Habibi, S., Collins, A.L., 2020. Mapping the spatial sources of atmospheric dust using GLUE and Monte Carlo simulation. *Science of the Total Environment* **723**, 138090. https://doi.org/10.1016/j.scitotenv.2020.138090.

Gong, H., Zhang, R., Yue, L., Zhang, Y.X., Li, J., 2015. Magnetic fabric from red clay sediments in the Chinese Loess Plateau. *Scientific Reports* **5**, 9706. https://doi.org/10.1038/srep09706.

Grousset, F.E., Biscaye, P.E., 2005. Tracing dust sources and transport patterns using Sr, Nd and Pb isotopes. *Chemical Geology* **222**, 149–167.

Gu, J.F., Zhu, C.J., Hao, Z.C., 2012. Application of principal component analysis in water quality evaluation by SPSS software. *Advanced Materials Research* **403**, 3277–3280.

Hu, W.J., Du, S.S., Tan, L.H., Chen, C.W., Duan, J.L., Wu, Y.Q., 2022. Provenance and formation mechanism of aeolian sands on the eastern bank of Co Nag Lake on the Qinghai-Tibet Plateau. *Catena* **208**, 105786. https://doi.org/10.1016/j.catena.2021.105786.

Jiang, Q.D., Yang, X.P., 2019. Sedimentological and geochemical composition of aeolian sediments in the Taklamakan Desert: implications for provenance and sediment supply mechanisms. *Journal of Geophysical Research: Earth Surface* **124**, 1217–1237.

Jickells, T.D., An, Z.S., Andersen, K.K., Baker, A.R., Bergametti, G., Brooks, N., Cao, J.J., *et al.*, 2005. Global iron connections between desert dust, ocean biogeochemistry, and climate. *Science* **308**(5718), 67–71.

Kang, C.G., Chang, Z., Cai, C.M., Jiang, H.J., Qiu, H., Ni, C., 2013. Heavy mineral characteristics of the loess deposits in the Eastern Songnen Plain: implication for sediment provenance. *Advanced Materials Research* **726**, 4081–4085.

Liang, A., Zhang, Z., Lizaga, I., Dong, Z., Zhang, Y., Liu, X., Xiao, F., Gao, J., 2023. Which is the dominant source for the aeolian sand in the Badain Jaran Sand Sea, Northwest China: fluvial or gobi sediments? *Catena* **225**, 107011. https://doi.org/10.1016/j.catena.2023.107011.

Licht, A., Pullen, A., Kapp, P., Abell, J., Giesler, N., 2016. Eolian cannibalism: reworked loess and fluvial sediment as the main sources of the Chinese Loess Plateau. *Geological Society of America Bulletin* **128**, 944–956.

Li, G., Chen, J., Ji, J., Yang, J., Conway, T.M., 2009. Natural and anthropogenic sources of East Asian dust. *Geology* **37**, 727–730.

Li, L., Chen, J., Chen, Y., Hedding, D.W., Li, T., Li, L.F., Li, G., *et al.*, 2018. Uranium isotopic constraints on the provenance of dust on the Chinese Loess Plateau. *Geology* **46**, 747–750.

Li, L., Li, G.K., Li, T., Yi, S., Lu, H., Hedding, D.W., Chen, J., Li, G., 2023. Tracking the provenance of aeolian loess in Northeastern China by uranium isotopes. *Geochemistry, Geophysics, Geosystems* **24**, e2022GC010715. https://doi.org/10.1029/2022GC010715.

Liu, J.H., Chi, Y.P., Xie, Y.Y., Kang, C.G., Wei, Z.Y., Wu, P., Sun, L., 2023. Geochemical characteristics of Songnen Sandy Land and its indication of contribution to aeolian dust. [In Chinese.] *Journal of Desert Research* **43**, 252–263.

Liu, L., Xie, Y.Y., Chi, Y.P., Kang, C.G., Wu, P., Wei, Z.Y., Zhang, Y.X., Zhang, M., 2021. Geochemical compositions of the Onqin Daga Sand Land and Horqin Sand Land and their implications for weathering, sedimentation and provenance. [In Chinese.] *Marine Geology & Quaternary Geology* **41**, 192–206.

Liu, Q., Yang, X., 2018. Geochemical composition and provenance of aeolian sands in the Ordos Deserts, northern China. *Geomorphology* **318**, 354–374.

Liu, T., Ding, Z., 1998. Chinese loess and the paleomonsoon. *Annual Review of Earth and Planetary Sciences* **26**, 111–145.

Liu, T.S., 1966. *Composition and Texture of Loess*. Science Press, Beijing.

Li, Y., Gholami, H., Song, Y., Fathabadi, A., Malakooti, H., Collins, A.L., 2020. Source fingerprinting loess deposits in Central Asia using elemental geochemistry with Bayesian and GLUE models. *Catena* **194**, 104808. https://doi.org/10.1016/j.catena.2020.104808.

Li, Y., Song, Y., Chen, X., Shi, Z., Kaskaoutis, D.G., Gholami, H., Li, Y., 2023. Late Pleistocene dynamics of dust emissions related to westerlies revealed by quantifying loess provenance changes in North Tian Shan, Central Asia. *Catena* **227**, 107101. https://doi.org/10.1016/j.catena.2023.107101.

Lizaga, I., Latorre, B., Gaspar, L., Navas, A., 2020. FingerPro: an R package for tracking the provenance of sediment. *Water Resources Management* **34**, 3879–3894.

Lu, H., An, Z., 1998. Paleoclimatic significance of grain size of loess-palaeosol deposit in Chinese Loess Plateau. *Science in China Series D: Earth Sciences* **41**, 626–631.

Maher, B.A., Prospero, J.M., Mackie, D., Gaiero, D., Hesse, P.P., Balkanski, Y., 2010. Global connections between aeolian dust, climate and ocean biogeochemistry at the present day and at the last glacial maximum. *Earth-Science Reviews* **99**, 61–97.

Mahowald, N.M., Kloster, S., Engelstaedter, S., Moore, J.K., Mukhopadhyay, S., McConnell, J.R., Albani, S., *et al.*, 2010. Observed 20th century desert dust variability: impact on climate and biogeochemistry. *Atmospheric Chemistry and Physics* **10**, 10875–10893.

Miyazaki, T., Kimura, J.I., Katakuse, M., 2016. Geochemical records from loess deposits in Japan over the last 210 kyr: lithogenic source changes and paleoclimatic indications. *Geochemistry, Geophysics, Geosystems* **17**, 2745–2761.

Nie, J., Peng, W., 2014. Automated SEM–EDS heavy mineral analysis reveals no provenance shift between glacial loess and interglacial paleosol on the Chinese Loess Plateau. *Aeolian Research* **13**, 71–75.

Prins, M.A., Vriend, M., Nugteren, G., Vandenberghe, J., Lu, H.Y., Zheng, H.B., Weltje, G.J., 2007. Late Quaternary aeolian dust input variability on the Chinese Loess Plateau: inferences from unmixing of loess grain-size records. *Quaternary Science Reviews* **26**, 230–242.

Pye, K., 1995. The nature, origin and accumulation of loess. *Quaternary Science Reviews* **14**, 653–667.

Qiu, S.W., 2008. *Geomorphology and Quaternary Geology and Application in Northeastern China*. Jilin Science and Technology Press, Changchun, pp. 114–124.

Rao, W.B., Tan, H.B., Jiang, S.Y., Chen, J.S., 2011. Trace element and REE geochemistry of fine-and coarse-grained sands in the Ordos deserts and links with sediments in surrounding areas. *Geochemistry* **71**, 155–170.

Rao, W.B., Yang, J.D., Chen, J., Li, G.J., 2006. Sr-Nd isotope geochemistry of eolian dust of the arid-semiarid areas in China: implications for loess provenance and monsoon evolution. *Chinese Science Bulletin* **51**, 1401–1412.

Shu, P., Li, B., Wang, H., Qiu, Y., Niu, D., Dianzhang, D., An, Z., 2018. Geochemical characteristics of surface dune sand in the Mu Us Desert, Inner Mongolia, and implications for reconstructing the paleoenvironment. *Quaternary International* **479**, 106–116.

Smalley, I., 1995. Making the material: the formation of silt sized primary mineral particles for loess deposits. *Quaternary Science Reviews* **14**, 645–651.

Song, Y., Chen, X., Li, Y., Fan, Y., Collins, A.L., 2022. Quantifying the provenance of dune sediments in the Taklimakan Desert using machine learning, multidimensional scaling and sediment source fingerprinting. *Catena* **210**, 105902. https://doi.org/10.1016/j.catena.2021.105902.

Sun, D.H., Bloemendal, J., Rea, D.K., An, Z., Vandenberghe, J., Lu, H., Su, R., Liu, T., 2004. Bimodal grain-size distribution of Chinese loess, and its palaeoclimatic implications. *Catena* **55**, 325–340.

Sun, D.H., Lu, H.Y., 2007. Grain size and dust accumulation rate of late Cenozoic eolian deposition and the inferred atmospheric circulation evolutions. [In Chinese.] *Quaternary Science* **2**, 251–262.

Sun, J.H., Xie, Y.Y., Kang, C.G., Chi, Y.P., Wu, P., Sun, L., Wei, Z.Y., Sun, Y., Hou, X.R., 2022. Stratigraphic properties of the Baitushan Formation in Pingan Town, the eastern foot of the Greater Hinggan Mountains: an indication of provenance and sedimentary environment. [In Chinese.] *Journal of Stratigraphy* **2**, 196–208.

Sun, J.M., 2002. Provenance of loess material and formation of loess deposits on the Chinese Loess Plateau. *Earth and Planetary Science Letters* **203**, 845–859.

Sun, J.M., Zhu, X.K., 2010. Temporal variations in Pb isotopes and trace element concentrations within Chinese eolian deposits during the past 8Ma: implications for provenance change. *Earth and Planetary Science Letters* **290**, 438–447.

Sun, L., Xie, Y.Y., Kang, C.G., Chi, Y.Y., Wu, P., Wei, Z.Y., Li, S., Zhao, Q., Liu, S., 2022. The composition of heavy minerals of the sandy lands, Northeast China and their implications for tracing detrital sources. *PLoS One* **17**, e0276494. https://doi.org/10.1371/journal.pone.0276494

Tamponi, M., Bertoli, F., Innocenti, F., Leoni, L., 2003. X-ray fluorescence analysis of major elements in silicate rocks using fused glass discs. *Atti della Società Toscana di Scienze Naturali, Memorie Serie A* **107**, 73–80.

Taylor, S.R., McLennan, S.M., 1985. *The Continental Crust: Its Composition and Evolution*. Oxford Blackwell, London.

Újvári, G., Kok, J.F., Varga, G., Kovács, J., 2016. The physics of wind-blown loess: implications for grain size proxy interpretations in Quaternary paleoclimate studies. *Earth-Science Reviews* **154**, 247–278.

Vandenberghe, J., 2013. Grain size of fine-grained windblown sediment: a powerful proxy for process identification. *Earth-Science Reviews* **121**, 18–30.

Wang, L.Y., Du, H.S., 2018. Dynamic evolution and simulation prediction of aeolian vegetation in Songnen Sandy Land in recent 35 years. [In Chinese.] *Research of Soil and Water Conservation* **25**, 380–385.

Wei, C.Y., Li, C.A., Kang, C.G., Chang, G.R., 2015. Grain size characteristics of Huangshan loess in Harbin and its implications for its genesis. *Earth Science* **40**, 1945–1954.

Wu, P., Xie, Y.Y., Li, Y., Kang, C.G., Chi, Y.P., Sun, L., Wei, Z.Y., 2022. Decoupling between circulation pattern and dust path since the last glacial in the Songnen Plain, NE China: insights from quantitative provenance reconstruction of the Harbin dust sediments. *Aeolian Research* **57**, 100818. https://doi.org/10.1016/j.aeolia.2022.100818.

Wu, P., Xie, Y.Y., Li, Y., Kang, C.G., Chi, Y.P., Sun, L., Wei, Z.Y., 2023. Provenance variations of the loess deposits in the East Asian monsoon boundary zone, Northeast China: response to the variations of climate and wind regimes. *Catena* **222**, 106804. https://doi.org/10.1016/j.catena.2022.106804.

Xie, J., Wu, F.Y., Ding, Z.L., 2007. Detrital zircon composition of U-Pb ages and Hf isotope of the Hunshandake sandland and implications for its provenance. *Acta Petrologica Sinica* **23**, 523–528.

Xie, Y.Y., Chi, Y.P., 2016. Geochemical investigation of dry- and wet-deposited dust during the same dust-storm event in Harbin, China: constraint on provenance and implications for formation of aeolian loess. *Journal of Asian Earth Sciences* **120**, 43–61.

Xie, Y.Y., Kang, C.G., Chi, Y., Du, H., Wang, J., Sun, L., 2019. The loess deposits in Northeast China: the linkage of loess accumulation and geomorphic-climatic features at the easternmost edge of the Eurasian loess belt. *Journal of Asian Earth Sciences* **181**, 103914. https://doi.org/10.1016/j.jseaes.2019.103914.

Xie, Y.Y., Kang, C.G., Chi, Y.P., Wu, P., Wei, Z.Y., Wang, J., Sun, L., 2020a. Reversal of the middle-upper Songhua River in the late Early Pleistocene, Northeast China. *Geomorphology* **369**, 107373. https://doi.org/10.1016/j.geomorph.2020.107373.

https://doi.org/10.1017/qua.2024.49 Published online by Cambridge University Press

Xie, Y.Y., Liu, L., Kang, C., Chi, Y., 2020b. Sr-Nd isotopic characteristics of the Northeast Sandy Land, China and their implications for tracing sources of regional dust. *Catena* **184**, 104303. https://doi.org/10.1016/j.catena.2019.104303.

Xie, Y.Y., Meng, J., Guo, L., 2014. REE geochemistry of modern eolian dust deposits in Harbin city, Heilongjiang province, China: implications for provenance. *Catena* **123**, 70–78.

Xie, Y.Y., Yuan, F., Zhan, T., Kang, C.G., Chi, Y.P., 2018. Geochemical and isotopic characteristics of sediments for the Hulun Buir Sandy Land, northeast China: implication for weathering, recycling and dust provenance. *Catena* **160**, 170–184.

Yang, P., Yuan, D., Yuan, W., Kuang, Y., Jia, P., He, Q., 2010. Formations of groundwater hydrogeochemistry in a karst system during storm events as revealed by PCA. *Chinese Science Bulletin* **55**, 1412–1422.

Yang, X., Li, H., Conacher, A., 2012. Large-scale controls on the development of sand seas in northern China. *Quaternary International* **250**, 74–83.

Yang, X., Liang, P., Zhang, D., Li, H., Rioual, P., Wang, X., Xu, B., *et al.* 2019. Holocene aeolian stratigraphic sequences in the eastern portion of the desert belt (sand seas and sandy lands) in northern China and their palaeoenvironmental implications. *Science China Earth Sciences* **62**, 1302–1315.

Yang, X., Liu, Y., Li, C., Song, Y., Zhu, H., Jin, X., 2007b. Rare earth elements of aeolian deposits in Northern China and their implications for determining the provenance of dust storms in Beijing. *Geomorphology* **87**, 365–377.

Yang, X., Zhu, B., White, P.D., 2007a. Provenance of aeolian sediment in the Taklamakan Desert of western China, inferred from REE and major-elemental data. *Quaternary International* **175**, 71–85.

Yue, Y., Wang, J., Lv, H., Liu, J., Wang, Z., Li, L., 2005. Land use optimization at ecological security level in desert regions – a case study of Horqin Sandy Land. *Progress in Safety Science and Technology* **5**, 2111–2116.

Zeng, M.X., Song, Y.G., Yang, H., Li, Y., Cheng, L., Li, F.Q., Zhu, L.D., Wu, Z.J., Wang, N.J., 2021. Quantifying proportions of different material sources to loess based on a grid search and Monte Carlo model: a case study of the Ili Valley, Central Asia. *Palaeogeography, Palaeoclimatology, Palaeoecology* **565**, 110210. https://doi.org/10.1016/j.palaeo.2020.110210.

Zhang, Q.Y., Zhao, X.Y., Zhang, Y., Li, L., 2002. Preliminary study on sand-dust storm disaster and countermeasures in China. *Chinese Geographical Science* **12**, 9–13.

Zhang, W.F., Zhao, J.X., Chen, J., Ji, J.F., Liu, L., 2018. Binary sources of Chinese loess as revealed by trace and REE element ratios. *Journal of Asian Earth Sciences* **166**, 80–88.

Zhang, Z.C., Liang, A.M., Dong, Z.B., Zhang, Z.H., 2022. Sand provenance in the Gurbantunggut Desert, northern China. *Catena* **214**, 106242. https://doi.org/10.1016/j.catena.2022.106242.

Zhang, Z.C., Pan, K.J., Zhang, C.X., Liang, A.M., 2020. Geochemical characteristics and the provenance of aeolian material in the Hexi Corridor Desert, China. *Catena* **190**, 104483. https://doi.org/10.1016/j.catena.2020.104483.

Zhao, W.C., Liu, L.W., Chen, J., Ji, J.F., 2019. Geochemical characterization of major elements in desert sediments and implications for the Chinese loess source. *Science China Earth Sciences* **62**, 1428–1440.

Zhao, Y.J., Song, C.W., 2021. The spatiotemporal evolution characteristics of the Songnen Sand Land's Net Primary Productivity (NPP). *Agriculture and Technology* **41**, 96–99.

https://doi.org/10.1017/qua.2024.49 Published online by Cambridge University Press